Ceramics International xxx (xxxx) xxx

Contents lists available at ScienceDirect

Ceramics International

journal homepage: www.elsevier.com/locate/ceramint

Microstructural development of platelet alumina while hot-pressing to transparency

Andrew P. Schlup, William J. Costakis Jr., Jeffrey P. Youngblood, Rodney W. Trice *

School of Materials Engineering, Purdue University, West Lafayette, IN, 47907, USA

ARTICLE INFO

Keywords:
Transparent alumina
Platelet-morphology
Hot-pressing
Crystallographic orientation

ABSTRACT

Transparent alumina specimens were produced using non-pre-aligned (NPA) and pre-aligned (PA) platelet alumina powder and hot-pressing at several different pressures. The effects of powder alignment and pressure on the crystallographic orientation, relative density, microstructure, and optical properties were studied. Additionally, samples were quenched at certain times during the hot-press run to investigate the microstructural evolution of the specimens. No significant trends were observed with increasing hot-pressing pressure. However, it is shown that while the pre-alignment procedure results in a higher degree of crystallographic orientation, the aligned platelets of the PA specimens result in a higher starting relative density, which causes faster densification to occur, yielding more grain-growth, porosity, and a lower final relative density. This ultimately results in minimal improvements in the in-line transmission compared to the NPA specimens, illustrating the importance of both high relative densities as well as crystallographic orientation for transparent alumina.

1. Introduction

Alumina is one of the most common technical ceramics due to its desirable properties (high hardness, high melting temperature, etc.) combined with its affordability. Additionally, alumina can be transparent at high relative densities (ρ>99.95%) [1,2], making it a promising candidate for ballistic applications that require transparency. However, the transparency of polycrystalline alumina is limited by its rhombohedral crystal structure [3], resulting in significant birefringent scattering from the refractive index mismatch at grain boundaries. A common way to minimize birefringent scattering in alumina is to utilize powder processing and sintering methods that result in a small grain size (<1.0 μm) [1,4], which reduces the scattering cross section of the grains and decreases the amount of light scattered at wide angles relative to the incident beam. Another way to minimize birefringent scattering is to process alumina such that the grains are aligned along the same crystallographic direction [5–10], which decreases the refractive index mismatch at the grain boundaries and reduces the angle that the light refracts as is passes across a grain boundary. This second approach has been explored by the present authors [11,12], where a platelet-morphology alumina powder was aligned using shear and elongational flows and densified via hot-pressing.

In a previous publication, hot-pressing parameters for non-pre-aligned platelet alumina powder (powder poured directly into the hot-press die) were explored [11] and optimal parameters resulted in a specimen with a high in-line transmission ($T_{ILT,645nm}$ = 65.3%) despite a large grain size (>60 μm). Costakis et al. [12] applied these optimal hot-pressing parameters to a pre-aligned platelet alumina specimen, resulting in an increased in-line transmission ($T_{ILT,645nm}$ = 70.0%) for similar grain sizes. This increase in the transparency is due to the pre-alignment procedure yielding a greater degree of crystallographic orientation, which further minimizes the refractive index mismatch. However, a density gradient near the outer edges of the specimen was observed [12]. Such a gradient is not desirable, as the properties of a transparent window used for ballistic applications [3,13,14] must be homogenous across its entire surface. Thus, there is motivation to identify optimal hot-pressing parameters for pre-aligned samples, as well as to investigate the microstructural development during hot-pressing.

The pressure applied during hot-pressing was previously identified as one of the key parameters for processing platelet alumina to transparency [11]. Specifically, it was found that too little pressure (≤5 MPa) would yield residual porosity due to insufficient driving force for densification, and too much pressure (≥20 MPa) would yield residual porosity due to a pore-swelling phenomenon. In both cases, the residual porosity results in scattering losses that minimize the in-line

* Corresponding author.
E-mail address: rtrice@purdue.edu (R.W. Trice).

https://doi.org/10.1016/j.ceramint.2021.10.031
Received 22 July 2021; Received in revised form 15 September 2021; Accepted 5 October 2021
Available online 7 October 2021

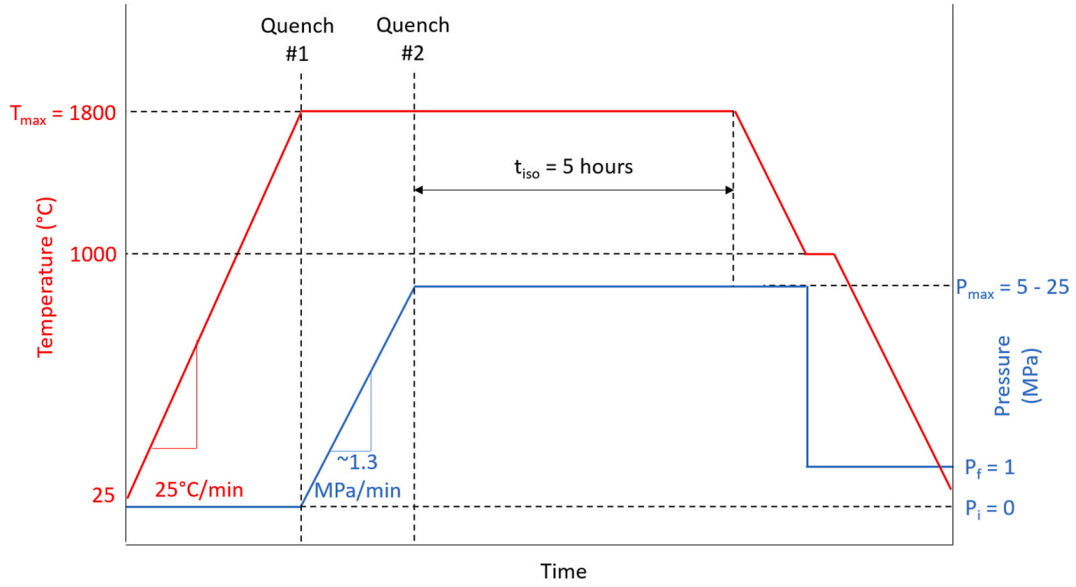

Fig. 1. Schematic illustrating the hot-pressing parameters and quench points.

transmission. A hot-pressing pressure of 10 MPa was identified as the optimal pressure. However, this was for non-pre-aligned platelet alumina. Costakis et al. [12] observed a density gradient in pre-aligned platelet alumina, which suggests that the state of the powder prior to hot-pressing affects the properties of the final sintered part, and that different hot-pressing parameters may be required to fully densify platelet alumina when it is in a pre-aligned state. It is thought that sufficient pressure, coupled with maintaining pressure during cooling, should result in samples with improved in-line transmission. Additionally, isothermal hold-time (the time held at maximum temperature and pressure) was identified as an important parameter [11]. It was found that 5 h was the minimum amount of time that results in adequate in-line-transmission. Therefore, 5 h is used in the current paper (instead of 7 h used previously) [12] with the goal of minimizing grain size.

In this work, platelet-morphology alumina powder that is randomly oriented (non-pre-aligned, NPA), as well as intentionally aligned (pre-aligned, PA), was hot-pressed at pressures ranging from 5 to 25 MPa. The effects that these parameters have on the crystallographic orientation, densification, microstructure, and optical properties of the specimens are discussed. In addition, samples were "quenched" at critical points during the hot-press run, capturing the microstructure at those points, allowing for investigation of the microstructural evolution of the specimens during hot-pressing.

2. Materials and methods

2.1. Powder preparation

RonaFlair® White Sapphire (Merck KGaA, EMD Performance Materials) platelet alumina powder was used. It has a platelet morphology, with a diameter and thickness of approximately 11 and 0.5 μm, respectively [11,12]. The platelet alumina powder was washed in high-purity de-ionized water by roller-milling for approximately 12 h, followed by centrifuging and decanting the water. The wash/centrifuge/decant process was repeated two additional times, followed by heating the powders at 110 °C for approximately 12 h in air to evaporate remaining water. Once dry, the platelet powder was sieved through a 250 μm nylon mesh to break apart soft agglomerates. 6.0 g of the sieved powder was poured directly into the hot-press die to ready the non-pre-aligned (NPA) specimens for hot-pressing.

The warm-pressing procedure developed by Costakis et al. [12] was used to obtain pre-aligned (PA) specimens. The raw platelet alumina powder (not water-washed) was blended at 130 °C in a thermoplastic polymer consisting of ethylene-ethyl-acrylate and plasticizers to form a 30 vol% solids-loading blend. The ceramic-filled polymer blend was pressed into a 38 × 76 × 17.9 mm preform, warm-pressed in a hydraulic press with heated platens (150 °C) to a thickness of ~0.5 mm with a load of 4500 kg, then slow-cooled to room temperature with the load maintained. Several 25.4 mm diameter discs were punched out of the pressed ceramic-filled polymer sheet, and 10 discs were stacked on top of each other to form an individual set of discs. Several sets of discs were placed on an alumina crucible and heated to 500 °C at 1.5 °C/h in flowing air to remove the fugitive polymer. Twenty of these burned-out disks (approximately 6.0 g total of pre-aligned platelet alumina powder) were carefully placed into the hot-press die to ready the PA specimens for hot-pressing.

2.2. Hot-pressing

The NPA and PA specimens were hot-pressed separately using a 25.4 mm inner diameter graphite die. Graphoil was applied to the graphite spacers, followed by boron nitride spray and molybdenum foil, to separate the powder bed from the graphite spacers. The graphite die was uniaxially cold-pressed at approximately 7 MPa to initially consolidate the powder. The assembled graphite die was placed in the hot-press (Centorr, Testorr™ series, mounted in an MTS, Model 312.21) and a vacuum was pumped for approximately 12 h, until a 45–55 millitorr (5.3–6.7 Pa) vacuum was achieved, and a vacuum of better than 170 millitorr (22.6 Pa) was maintained from room temperature to 1550 °C. At 1550 °C, the vacuum was switched off and the furnace chamber was backfilled with high-purity gettered nitrogen, which continuously flowed at approximately 4 L/min and 2 psi (1.4×10^4 Pa) for the remainder of the hot-press run. Fig. 1 illustrates the temperature and loading profile used during the hot-press runs. At room temperature, the top platen of the load frame was positioned ~5 mm away from the top ram of the assembled hot-press die, allowing the die to expand freely during heating at a rate of 25 °C/min to the maximum temperature of 1800 °C. When the furnace reached the maximum temperature, the hot-pressing pressure (P_{max}, 5–25 MPa) was applied at a rate of 1.3 MPa/min. Once the pressure was achieved, the temperature and P_{max} were held constant for 5 h. The P_{max} was maintained during cooling (25 °C/min) to 1000 °C. At 1000 °C, the pressure was quickly reduced to 1 MPa, and the temperature was held at 1000 °C for 10 min to relieve residual stresses [15] before continuing cooling to room temperature. Load and

ram displacement were recorded throughout the run.

In addition to the typical hot-pressed specimens, NPA and PA specimens were "quenched" in order to capture the microstructure at certain points during the hot-press run. This was done by preparing additional specimens in the same manner as a typical hot-press run and heating the hot-press up to temperature (1800 °C), but the entire system was shut-down at two different points, as illustrated in Fig. 1. The Quench #1 point was immediately after reaching the maximum temperature of 1800 °C, but before any pressure is applied. The Quench #2 point was immediately after a pressure of 20 MPa was applied. For both quench points, the furnace power was shut off, allowing un-controlled cooling to room temperature. For the second quench point, the pressure was immediately removed at the moment of system shut-down.

2.3. Specimen polishing, density, orientation, and microscopy characterization

Hot-pressed specimens were ground and polished to minimize surface scattering. A 150-grit metal-bonded diamond grinding wheel was used to machine equal amounts of material from each side of the specimens to a thickness of approximately 1.5 mm. Both sides of the specimens were polished using progressively finer diamond suspensions, ending with a 1 μm diamond suspension, resulting in final specimen thicknesses ranging from 1.22 to 1.29 mm.

The densities of the hot-pressed and Quench #2 specimens were measured using the Archimedes method [16]. A commercially available single-crystal sapphire transparent standard was measured alongside the hot-pressed specimens and yielded a density of 3.985 g/cm^3. The geometric densities of the Quench #1 specimens were measured by carefully machining into a cylindrical shape and measuring the dimensions and mass. Relative densities of the specimens were calculated by dividing their density by the density of the single-crystal sapphire standard.

The crystallographic orientation of the hot-pressed specimens was determined via rocking curve analysis on the (000.12) plane using a Panalytical Empyrean Diffractometer (Malvern Panalytical Ltd, Royston, UK). The exact methods and specifications are discussed elsewhere [12]. Briefly, an omega scan (rocking curve tilt) was performed on the Bragg's peak that corresponds to the (000.12) plane ($2\theta = 90.6°$). Three separate rocking curves were performed on each side of the specimens to obtain statistical data. An orientation parameter "*r*" was obtained from the curve fit of the March-Dollase equation [12]. The *r* value approaches zero (0) for perfect orientation (e.g. single crystal sapphire), while a value of one (1) indicates no orientation (e.g. polycrystalline ceramic).

Cross-sections of the specimens were characterized via scanning electron microscopy (SEM). The hot-pressed specimens were sectioned and polished to a 1 μm diamond finish, and thermally etched at 1600 °C for 30 min in air. The specimens were sputter-coated with Au-Pd, and the microstructures were observed by SEM with a FEI Quanta650 at 15 kV. Line intercept analysis was performed, obtaining at least 200 intersections. The average intercept length was multiplied by the geometric factor 1.56 to obtain the average grain size.

The Quench #1 specimens required a different procedure to obtain microstructures, due to their low relative density ($\rho<40\%$) and fragile nature. As such, they were carefully sectioned with a metal saw blade and dry "polished" by hand using progressively finer silicon-carbide paper, ending with 4000-grit. Residual powder was removed from the "polished" surface with compressed air, sputter-coated with Au-Pd, and the microstructures were observed with a Phenom Desktop SEM.

2.4. Optical measurements

Optical measurements were made using a PerkinElmer Lambda 950 UV-VIS-NIR spectrophotometer equipped with an integrating sphere. Wavelengths ranging from 200 to 800 nm were measured using a photomultiplier tube detector. A wavelength of 645 nm was chosen as the representative value for optical properties in the present study, which is a similar wavelength used in the literature [1,17,18]. Total transmission, in-line transmission, reflection, and absorption were measured using the spectrophotometer, and the forward and backward scattering were derived from them. The optical properties were normalized to a thickness of 0.8 mm. The exact measurement methods, calculations, and thickness normalization are described elsewhere [11].

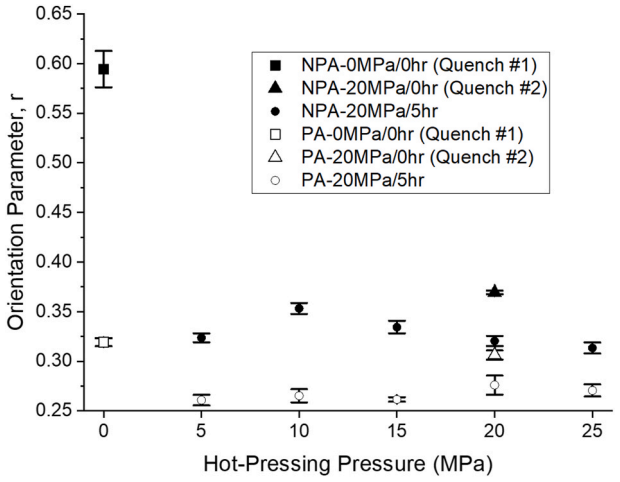

Fig. 2. Orientation parameter "*r*" as a function of pressure for NPA and PA specimens during key points during the hot-press run.

3. Results and discussion

3.1. Crystallographic orientation

The orientation parameter, *r*, as a function of hot-pressing pressure is shown in Fig. 2. The non-pre-aligned (NPA, closed shapes) specimens have a higher *r* than the pre-aligned (PA, closed shapes) specimens, indicating that the NPA specimens have a lesser degree of crystallographic orientation than the PA specimens. The previous investigation by Costakis et al. [12]. showed that the pre-alignment procedure is effective in preferentially aligning the platelets parallel to the direction of polymer flow. Fig. 2 supports the Costakis et al. work and indicates that the pre-alignment process, when paired with hot-pressing, is able to repeatedly achieve higher crystallographic orientation than NPA platelet alumina.

Fig. 2 shows that higher pressures have no significant effect on the crystallographic orientation of NPA and PA specimens hot-pressed for 5 h (circles). For NPA specimens (closed circles), there appears to be a slight decrease in *r* with increasing pressure, particularly between 10 and 25 MPa. This could be due to higher pressures resulting in more particle-rearrangement, though it is not clear if this trend is significant, especially when the outlier at 5 MPa is considered. For PA specimens (open circles), it is evident that increasing hot-pressing pressure has no significant effect on *r*. This is likely due to the pre-alignment procedure having already aligned the platelets the maximum amount, and higher pressures do not result in any additional particle-rearrangement.

Fig. 2 does, however, indicate that there is a noticeable effect on the crystallographic orientation at the different quench points. The *r* of the NPA specimen quenched before any pressure was applied (Quench #1, closed square) is high, while the *r* of the NPA specimen after 20 MPa is applied (Quench #2, closed triangle) is significantly lower. This shows that simply pouring the platelet alumina powder directly into the hot-press die results in a very low degree of crystallographic alignment (high *r* at Quench #1), and the pressure-application step during the hot-press run drastically increases the alignment (lower *r* at Quench #2). This is likely due to particle-rearrangement, where the application of pressure causes the (mostly) randomly oriented platelets to rotate into a

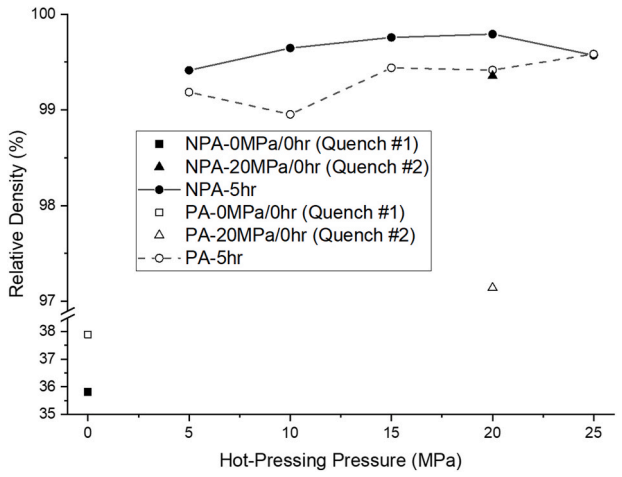

Fig. 3. Relative density as a function of hot-pressing pressure for the NPA and PA specimens at key points during the hot-press run.

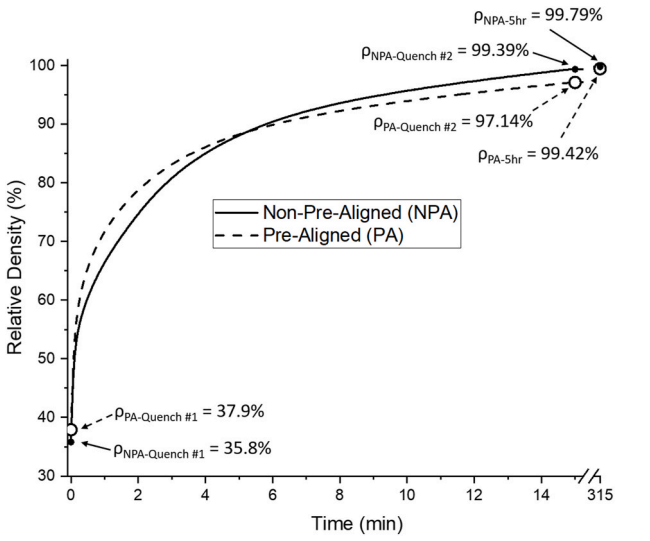

Fig. 4. Relative density as a function of time for the NPA and PA specimens at each of the key points during the hot-press run.

flatter, more geometrically favorable, orientation. Furthermore, holding for an additional 5 h (closed circle) results in a further decrease in *r*, meaning that additional crystallographic alignment is occurring during the isothermal hold at maximum temperature and pressure. A similar trend is observed for the PA specimens (open square for Quench #1, and open triangle for Quench #2), though to a lesser degree. As previously mentioned, this is likely due to the pre-alignment procedure having already oriented the platelets prior to hot-pressing.

3.2. Relative density

Fig. 3 shows the relative density of NPA and PA specimens as a function of hot-pressing pressure. There does not appear to be a significant trend in the relative density with increasing pressure, especially considering the fluctuation at 25 MPa for NPA and at 10 MPa for PA. However, the difference in relative density between the NPA and PA samples is significant. Specifically, the relative density of the NPA specimens (closed circles, solid line) is higher than the PA specimens (open circles, dotted line) at all hot-pressing pressures except for $P_{max} =$ 25 MPa. This result suggests that the state of the platelet alumina powder prior to hot-pressing has a significant effect on the densification behavior.

Fig. 3 also shows the relative densities of NPA and PA specimens quenched at 0 MPa (Quench #1, squares) and 20 MPa (Quench #2, triangles). The relative densities of the Quench #1 specimens are very low ($\rho<40\%$), then increases to $\rho>97\%$ for the Quench #2 specimens. The low density at Quench #1 is because the platelets have a very large diameter (11 μm), which yields very low driving forces for densification, and the powder-beds will not densify during heating with no applied pressure. When the pressure is applied (Quench #2), there is now sufficient driving force for densification, resulting in the significant increase in density of the Quench #2 specimens. It is important to note that the relative density of the NPA-0MPa/0hr specimen (Quench #1, closed square) is lower than the relative density of the PA-0MPa/0hr specimen (Quench #1, open square). It is thought that the NPA-0MPa/0hr specimen has a lower relative density because the platelet powder is simply poured into the hot-press die, and the high aspect-ratio of the platelets inhibits efficient packing. Conversely, the PA-0MPa/0hr specimen has a higher relative density because the high aspect-ratio platelets are arranged into a more organized, "brick-like" packing structure due to the pre-alignment procedure. This behavior is briefly discussed by Reed [19], where anisometric particles will produce a higher packing density when oriented along the same direction, yielding a lower porosity and smaller range of pore sizes.

Another important result in Fig. 3 is that the relative densities of the NPA and PA Quench #1 specimens switch after the hot-pressing pressure of 20 MPa (Quench #2) is applied: the NPA-20MPa/0hr (Quench #2, closed triangle) specimen now has a higher relative density than the PA-20MPa/0hr (Quench #2, open triangle) specimen. This result in unexpected, as higher starting densities will generally result in higher final densities when processing ceramics [19,20]. To more clearly illustrate the changes in density at these different quench points, the relative density as a function of time for the PA and NPA specimens are shown in Fig. 4. This curve was created by mathematically relating the starting (Quench #1) and ending (Quench #2) relative densities to the recorded displacement during hot-pressing. This was done using a law of averages approach, as shown in Equation (1):

$$\rho_t = \rho_1(1-\varepsilon_t) + \rho_2\varepsilon_t \quad (1)$$

Where ρ_t is the relative density at time t, ρ_1 is the relative density at Quench #1, and ρ_2 is the relative density at Quench #2. ε_t is the strain at time t, and is given by Equation (2):

$$\varepsilon_t = \frac{d_f - d_t}{d_f} \quad (2)$$

Where d_t is the displacement at time t and d_f is the final displacement.

Fig. 4 shows that the NPA specimen starts at a lower relative density than the PA specimen. During the first few minutes of pressure-application, the NPA specimen densifies at a slower rate than the PA specimen. After approximately 5 min, the relative density of the NPA specimen surpasses the PA specimen and reaches 99.39% at the Quench #2 point ($P_{max} = 20$ MPa), which is 2.25% higher than the PA specimen. After an additional 5 h, the NPA and PA specimens further densify to their final relative densities of 99.79% and 99.42%, respectively. It is evident that the NPA specimen densifies more slowly than the PA specimen at the onset of pressure application because the NPA specimen starts at a lower relative density. This is a commonly understood trend in ceramic processing, as a lower relative density means that there are fewer particle-particle interfaces to facilitate in grain boundary diffusion and subsequent densification [19,20]. However, the NPA specimen continues to densify to a higher relative density than the PA specimen. The reason for this is not immediately apparent and is discussed in the next section.

3.3. Microstructure

The microstructures near the centers of NPA and PA specimens at the

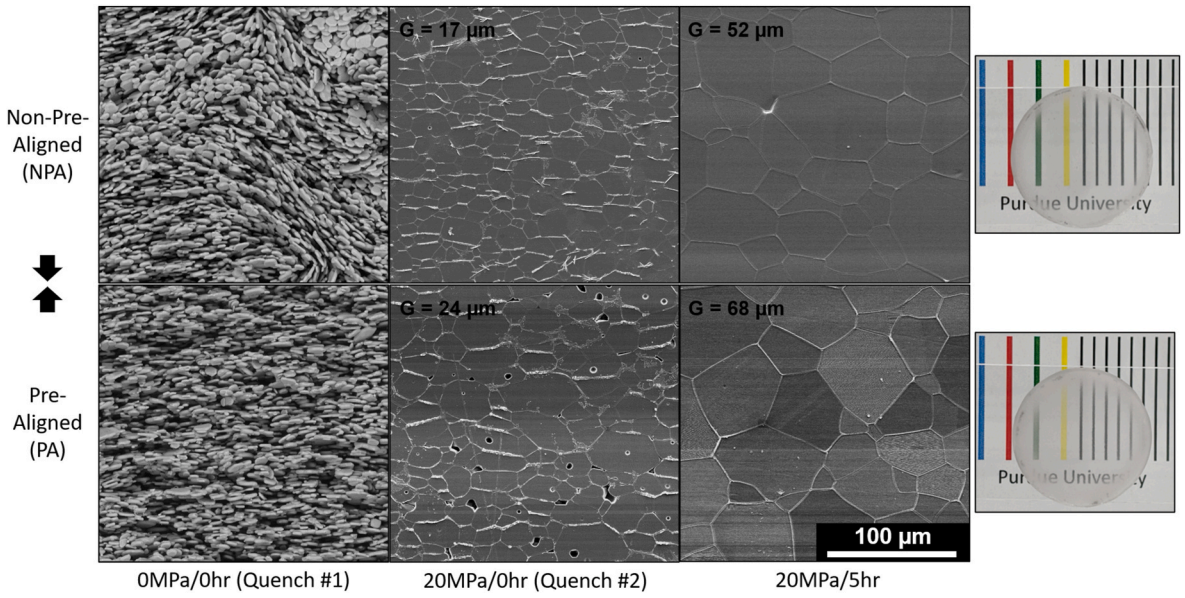

Fig. 5. SEM micrographs of the centers of Non-Pre-Aligned (NPA) and Pre-Aligned (PA) specimens during various steps during the hot-press run. The arrows indicate the hot-pressing direction, and to the right are macroscale images of the PA-20MPa/5hr specimens placed 2 cm above the text.

different quench points, as well as the fully processed specimens, are shown in Fig. 5. For both powder-types, the Quench #1 specimen is very porous, as confirmed by their low relative densities (Figs. 3 and 4). Additionally, the diameter of the platelets is approximately 10 μm, relatively unchanged from the original diameter of the raw platelets. However, the thickness of the platelets appears to have increased from ~0.1 μm to ~2.0 μm. The reason for this is unknown, though it is speculated that platelets that were initially in direct basal-plane contact with each other may have grown into each other, forming a single, thicker platelet. The most noticeable difference between the powder-types at the Quench #1 point is the difference in microstructural alignment. The NPA specimen appears to be mostly randomly oriented throughout, though there are regions of local alignment. This random orientation is confirmed by the high r in Fig. 2. The PA specimen, on the other hand, has a much greater degree of microstructural alignment throughout the entire specimen. This high degree of alignment is similarly confirmed by the low r in Fig. 2 and is expected due to the pre-alignment procedure.

A different microstructure is observed at the Quench #2 point for both powder-types. The relative density of the specimens increases, the grain size increases, and the microstructures still exhibit morphological orientation, though at a much lower aspect ratio compared to the Quench #1 point. Additionally, there is a whitish-colored phase at the grain boundaries. This whitish-colored phase was confirmed to be calcium impurities by EDS. Impurity measurements indicated that approximately 0.012% of calcium impurities are present in the RonaFlair® platelet alumina powder [11]. While the supplier does not disclose the production method of the RonaFlair® platelets, it is known that a calcium oxide (CaO) and silicon oxide (SiO_2) glassy phase can promote anisotropic grain grown of alumina [21], so it is possible that the supplier uses a similar composition to produce the high aspect-ratio platelets. If this is the case, this could be the source of the residual calcium impurities, except there is not enough of the calcium phase to continue to promote anisotropic grain growth during hot-pressing. Instead, the grain-growth begins to occur along the c-axis of the alumina platelets, resulting in the more equiaxed morphology that is observed in these microstructures.

There is a visible difference in the amount of grain growth and porosity of the NPA and PA Quench #2 microstructures. The NPA Quench #2 specimen exhibits minimal grain growth compared to its previous state (Quench #1), as well as minimal porosity. The PA Quench #2 specimen, on the other hand, exhibits noticeable grain growth compared to its previous state (Quench #1), as well as significant inter and intra-granular porosity.

After hot-pressing at a maximum temperature of 1800 °C and a hot-pressing pressure of 20 MPa for an additional 5 h, the NPA and PA specimens (20MPA/5hr) undergo further change, as shown in Fig. 5. First, there is virtually no porosity and the grain size drastically increases, which is to be expected at this temperature for this amount of time [19]. Second, the grains appear to be even more equiaxed than what was observed in the respective Quench #2 microstructures. Finally, the calcium impurities (whitish-colored phase along the grain boundaries) qualitatively appear to have diminished, though this could be attributed to the edge effect at the grain boundary, so further analysis is required to confirm this.

The microstructures in Fig. 5, along with the orientation and density data given in the earlier figures, allow for postulation as to why the NPA specimens reaches a higher final relative density than the PA specimens. Fig. 2 shows that the NPA specimens are more randomly oriented prior to the application of pressure. It is because of this random orientation that the starting relative density of the NPA specimens is lower than the PA specimens (Figs. 3 and 4). Because the NPA specimen starts at a lower relative density than the PA specimen, it densifies at a slower rate during the initial stages of the application of pressure (Fig. 4). Then, it is because of this slower densification rate that there is less grain growth in the NPA specimen (Fig. 5). It is generally understood that a slower densification rate will result in slower grain-growth rates, and subsequently result in less porosity [19,20]. The microstructural differences between the NPA and PA specimens at the Quench #2 point confirm this, where the NPA specimen has a smaller grain size and minimal porosity, while the PA specimen has a larger grain size and significant porosity, resulting in the higher relative density of the NPA specimen at this quench point.

The differences observed at the Quench #2 point explain the differences that are observed in the final microstructures (20MPa/5hr). Namely, the NPA specimen has a smaller final grain size than the PA specimen. The NPA specimen has no visible porosity at this stage, which is to be expected based on the lack of porosity of its previous stage, but it is interesting that the PA specimen also has no visible porosity at this stage, especially considering the differences in relative density (Figs. 3 and 4). However, the reader is reminded that these microstructures were obtained from the center of the specimens, and the edges of the

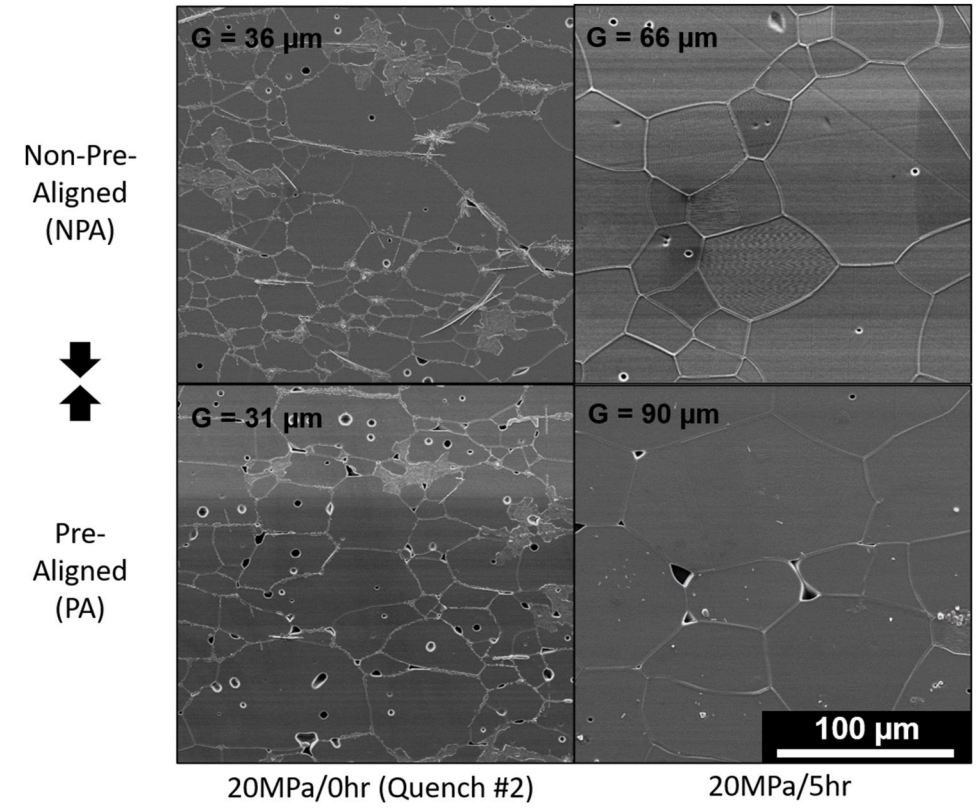

Fig. 6. SEM micrographs of the edges of the Non-Pre-Aligned (NPA) and Pre-Aligned (PA) specimens. The arrows indicate the hot-pressing direction.

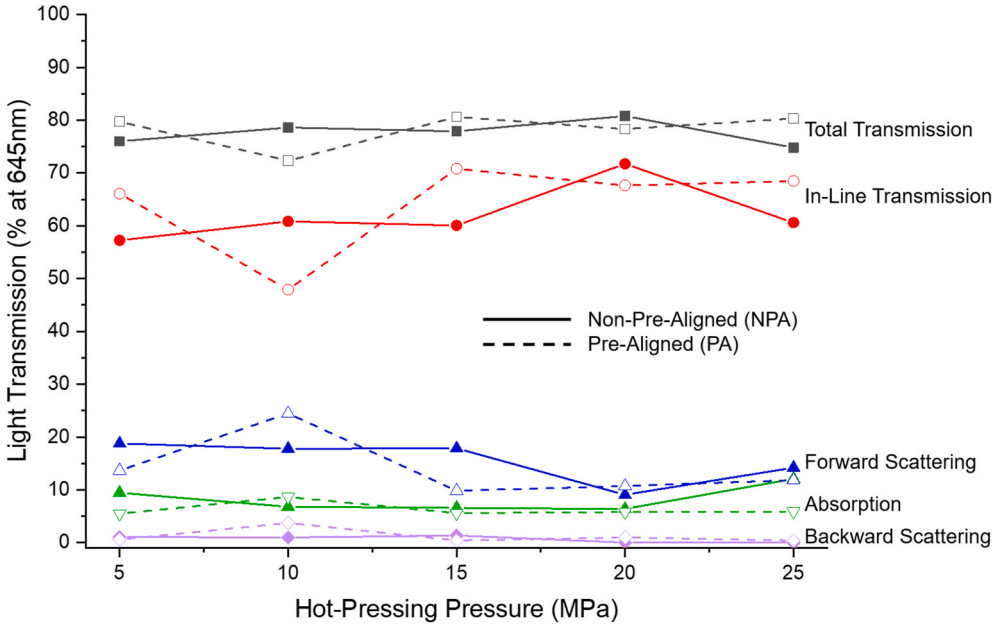

Fig. 7. Light transmission as a function of hot-pressing pressure for NPA and PA specimens. Values taken at a wavelength of 645 nm and normalized to a thickness of 0.8 mm.

specimens will have noticeable porosity, which is confirmed in the micrographs shown in Fig. 6. Specifically, the few small intragranular pores in the edges of the NPA specimen is minimal compared to the few large intergranular pores of the PA specimen and explains why the NPA specimen has a higher relative density than the PA specimen. Another interesting feature in Fig. 5 is that the intragranular pores of the final PA specimen (20MPa/5hr) have a concave morphology, which means that the pores are still able to shrink and further densify [20]. This suggests that a longer isothermal hold time may result in further densification.

Another explanation for why the NPA specimens result in a higher relative density than the PA specimens is the possible occurrence of primary recrystallization during the application of pressure. This mechanism was discussed in the previous publication [11], and is the primary mechanism suggested by Heuer et al. in their work on

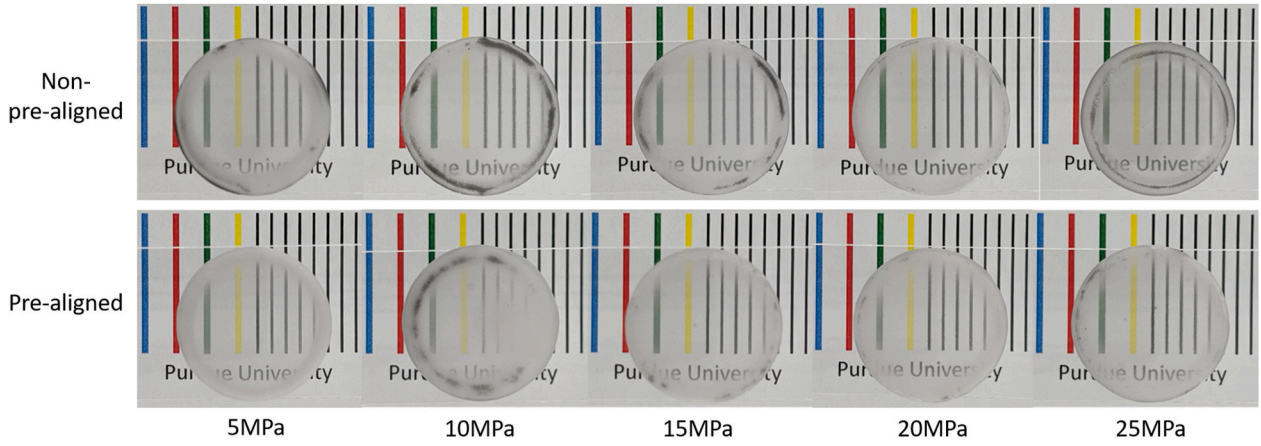

Fig. 8. Macroscale images of NPA and PA specimen hot-pressed at the different hot-pressing pressures, illustrating transparency and the density gradients. Specimens are placed 2 cm above the text.

transparent alumina produced by sinter-forging [5–7,22,23]. Heuer et al. suggested that a sufficient amount of deformation must occur in the specimen during sinter-forging in order to induce primary recrystallization, and that more deformation generally resulted in higher densities and a greater degree of crystallographic orientation [7]. It is possible that a similar mechanism is occurring in the current paper, where the NPA specimens start at a lower relative density than the PA specimens, allowing them to undergo more deformation during the application of pressure, resulting in more primary recrystallization and a higher final relative density. However, this is for platelet-morphology alumina, whereas the primary recrystallization described by Heuer et al. was seen with equiaxed-morphology alumina. Further examination is required to confirm if primary recrystallization is occurring in the current specimens.

3.4. Optical properties

The optical properties (total/in-line transmission, forward/backward scattering, and absorption) of NPA and PA specimens hot-pressed at different pressures are shown in Fig. 7. There is no noticeable trend in the optical properties with an increase in pressure, which is different to what was observed in a previous publication [11], where it was shown that too high or too low of a hot-pressing pressure resulted in lower T_{ILT}. Higher pressure yielding lower T_{ILT} was explained by a pore-swelling phenomenon, in which the internal pressure of the pores causes the surrounding matrix to creep when the hot-pressing pressure is removed prior to cooling from 1800 °C, resulting in more porosity and lower T_{ILT}. In the current work, this hypothesis was tested by maintaining hot-pressing pressure until cooling to 1000 °C. It was thought that maintaining the hot-pressing pressure until the system is sufficiently cooled would allow the alumina to retain a smaller pore size, as the surrounding matrix would be unable to creep from the pore pressure and swell to a lower relative density. As shown in Fig. 7, maintaining pressure during cooling resulted in a higher in-line transmission for all specimens, with minimal changes due to increasing pressure. Additionally, the in-line transmission is at least 60% for both powder-types at $P_{max} \geq 15$ MPa. This was not the case in the previous publication [11], where the in-line transmission was less than 55% at $P_{max} \geq 20$ MPa, which further suggests that maintaining pressure during cooling helps to maintain high relative densities and improving transparency by reducing pore size.

An important feature of Fig. 7 is that there is no noticeable difference in the optical properties between the NPA and PA specimens. This was not expected, as the crystallographic orientation should improve the in-line transmission, as illustrated in a previous publication [12]. The lack of optical difference between sample types is explained by the differences in crystallographic orientation and relative density. Specifically, the NPA specimens have a lower degree of crystallographic orientation (Fig. 2) and a higher relative density (Figs. 3 and 4), while the exact opposite is the case for the PA specimens: They have a higher degree of crystallographic orientation and a lower relative density. This means that any optical improvements that the PA samples might have due to crystallographic orientation are diminished by their lower relative density, which comes about as a result of their densification behavior, as discussed in the previous section. This relationship between crystallographic orientation and relative density emphasizes the importance of both microstructural properties, and how they relate to the resulting optical properties.

The differences in final grain size between the NPA and PA specimens can also explain why there is a minimal difference in the optical properties, despite the notable difference in crystallographic orientation. As shown in Fig. 5, the grain size of the final NPA specimen is 52 μm, whereas the grain size of the final PA specimen is 68 μm. It is well-known that birefringent ceramics with a smaller grain size will have a higher in-line transmission than those with a larger grain size, as shown by the Raleigh-Gans-Debye model developed by Apetz et al. [1] This model establishes that the refractive index mismatch (Δn) is very important, and is directly influenced by crystallographic orientation, but the grain size is equally important. Therefore, while the PA specimens have a higher degree of crystallographic orientation (low r in Fig. 2, which translates to a lower Δn), their in-line transmission is diminished by their larger grain size, and vice/versa for the NPA specimens. This further explains why there is minimal difference in the optical properties of the NPA and PA specimens, and illustrates the importance of both grain size and crystallographic orientation in birefringent transparent ceramics.

The NPA specimen hot-pressed at $P_{max} = 20$ MPa exhibited an in-line transmission of $T_{ILT,645nm} = 71.7\%$, while the similar PA specimen is $T_{ILT,645nm} = 67.6\%$, which is only 4.1% lower than the NPA specimen. However, the in-line transmission of this PA specimen is not as high as the specimen produced by Costakis et al., where a value of $T_{ILT,645nm} = 70.0\%$ was achieved at $P_{max} = 10$ MPa [12]. The higher in-line transmission at a lower pressure observed by Costakis is easily explained by the longer isothermal hold time that was used: 7 h, instead of the 5 h used in the current study. The additional 2 h at max temp and pressure appears to effectively densify the PA specimen, despite the densification issues that arise with the PA specimens, as discussed in the previous section. This suggests that a longer isothermal hold time is critical to fully densify a specimen prepared via hot-pressing pre-aligned platelet alumina.

Finally, Fig. 8 shows macroscale images of the hot-pressed specimens. For all specimens, an area of lower density was observed in the

form of a whitish color around the outer perimeters and is more prominent in the PA specimens. This density gradient is similar to what was observed by Costakis et al. [12], and is confirmed by the differences in porosity observed in the microstructures at the centers (Fig. 5) and edges (Fig. 6) of the specimens. These density gradients qualitatively appear to be diminishing at higher pressures, suggesting that pressures higher than the ones used in this study could potentially minimize or even eliminate this defect.

4. Conclusions

Transparent alumina specimens were hot-pressed using non-pre-aligned (NPA) and pre-aligned (PA) platelet alumina powder. The PA specimens exhibited higher crystallographic orientation at all stages of hot-pressing, confirming that the warm-pressing procedure is effective at aligning the platelets along the same crystallographic direction. The NPA specimens exhibited a higher relative density than the PA specimens, and no significant increase in relative density at higher pressures. Quenching the specimens at certain times during the hot-press run reveal that the NPA specimens start at a lower initial relative density compared to the PA specimens, which results in less grain growth and porosity. This difference in the densification behavior explains why there is a minimal difference in the in-line transmission between the NPA and PA specimens, despite the NPA specimens having a lesser degree of crystallographic orientation. Improvements in optical properties due to crystallographic orientation may only be realized at sufficient relative densities, suggesting that longer isothermal hold times and higher pressures than those used in the current study are necessary to fully densify specimens produced using pre-aligned platelet alumina.

Declaration of competing interest

The authors declare that they have no known competing financial interests or personal relationships that could have appeared to influence the work reported in this paper.

Acknowledgments

This study was financially supported by the Army Research Office (Grant #W911NF-17-1-0203), with Dr. Michael Bakas Program Manager. The authors would like to thank Monica Gehrich and Adam Smith for help with specimen processing, and Merck KGaA (EMD Performance Materials) for providing the RonaFlair® platelet alumina powder used in this research.

References

[1] R. Apetz, M.P.B. Van Bruggen, Transparent alumina : a light-scattering model, J. Am. Ceram. Soc. 86 (2003) 480–486.
[2] J.G.J. Peelen, Light transmission of sintered alumina, Philips Tech. Rev. 36 (1976) 47–52.
[3] D.C. Harris, L.F. Johnson, L.R. Cambrea, L. Baldwin, M. Baronowski, D.E. Zelmon, W.B. Poston, J.D. Kunkel, M. Parish, M.R. Pascucci, J.J. Gannon, T.-C. Wen, Refractive index of infrared-transparent polycrystalline alumina, Wind. Dome Technol. Mater. XV (2017), https://doi.org/10.1117/12.2257580.
[4] K. Hayashi, O. Kobayashi, S. Toyoda, K. Morinaga, Transmission optical properties of polycrystalline alumina with submicron grains, Mater. Trans., JIM 32 (1991) 1024–1029, https://doi.org/10.2320/matertrans1989.32.1024.
[5] W.H. Rhodes, D.J. Sellers, T. Vasilos, Hot-Working of aluminum oxide: II, optical properties, J. Am. Ceram. Soc. 58 (1974) 31–34.
[6] W.H. Rhodes, D.J. Sellers, A.H. Heuer, T. Vasilof, Development and Evaluation of Transparent Aluminum Oxide, Lowell, MA, 1967.
[7] A.H. Heuer, D.J. Sellers, W.H. Rhodes, Hot working of aluminum oxide. 1: primary recrystallization and texture, J. Am. Ceram. Soc. 52 (1969) 468–474.
[8] X. Mao, S. Wang, S. Shimai, J. Guo, Transparent polycrystalline alumina ceramics with orientated optical axes, J. Am. Ceram. Soc. 91 (2008) 3431–3433, https://doi.org/10.1111/j.1551-2916.2008.02611.x.
[9] H. Yi, X. Mao, G. Zhou, S. Chen, X. Zou, S. Wang, S. Shimai, Crystal plane evolution of grain oriented alumina ceramics with high transparency, Ceram. Int. 38 (2012) 5557–5561, https://doi.org/10.1016/j.ceramint.2012.03.074.
[10] T. Ashikaga, B.N. Kim, H. Kiyono, T.S. Suzuki, Effect of crystallographic orientation on transparency of alumina prepared using magnetic alignment and SPS, J. Eur. Ceram. Soc. 38 (2018) 2735–2741, https://doi.org/10.1016/j.jeurceramsoc.2018.02.006.
[11] A.P. Schlup, W.J. Costakis, W. Rheinheimer, R.W. Trice, J.P. Youngblood, Hot-pressing platelet alumina to transparency, J. Am. Ceram. Soc. 103 (2020) 2587–2601, https://doi.org/10.1111/jace.16932.
[12] W.J. Costakis, A.P. Schlup, J.P. Youngblood, R.W. Trice, Aligning α-alumina platelets via uniaxial pressing of ceramic-filled thermoplastic polymer blends for the improvement of final sintered transparency, J. Am. Ceram. Soc. 103 (2020) 3500–3512, https://doi.org/10.1111/jace.17044.
[13] A. Krell, J. Klimke, T. Hutzler, Transparent compact ceramics: inherent physical issues, Opt. Mater. 31 (2009) 1144–1150, https://doi.org/10.1016/j.optmat.2008.12.009.
[14] A. Krell, J. Klimke, T. Hutzler, Advanced spinel and sub-μm Al2O3 for transparent armour applications, J. Eur. Ceram. Soc. 29 (2009) 275–281, https://doi.org/10.1016/j.jeurceramsoc.2008.03.024.
[15] B.N. Kim, K. Hiraga, K. Morita, H. Yoshida, T. Miyazaki, Y. Kagawa, Microstructure and optical properties of transparent alumina, Acta Mater. 57 (2009) 1319–1326, https://doi.org/10.1016/j.actamat.2008.11.010.
[16] ASTM International, ASTM Standard C693, 1993 (2013) Standard Test Method for Density of Glass by Buoyancy, https://doi.org/10.1520/C0693-93R13.2, 2013.
[17] A. Krell, P. Blank, H. Ma, T. Hutzler, M.P.B. Van Bruggen, R. Apetz, Transparent sintered corundum with high hardness and strength, Am. Ceram. Soc. 86 (2003) 12–18.
[18] A. Pringuet, T. Takahashi, S. Baba, Y. Kamo, Z. Kato, K. Uematsu, S. Tanaka, Fabrication of transparent grain-oriented polycrystalline alumina by colloidal processing, Am. Ceram. Soc. 99 (2016) 3217–3219, https://doi.org/10.1111/jace.14476.
[19] J.S. Reed, Principles of Ceramics Processing, second ed., 1995.
[20] M.N. Rahaman, Ceramic Processing and Sintering, second ed., 2003.
[21] M. Seabaugh, G.L. Messing, Texture development by templated grain growth in liquid-phase-sintered alpha-alumina, J. Am. Ceram. Soc. 88 (1997) 1181–1188.
[22] A.H. Heuer, W.H. Rhodes, D.J. Sellers, T. Vasilos, Microstructure Studies of Polycrystalline Refractory Oxides, 1967.
[23] W.H. Rhodes, Microstructure Studies of Polycrystalline Refractory Compounds, 1974.